

THE PERFORMANCE OF THE ZEUS CALORIMETER*

JAMES A. CRITTENDEN

*Physikalisches Institut, Universität Bonn
Nußallee 12, D-53115 Bonn, Germany*

for

The ZEUS Calorimeter Group

ABSTRACT

The ZEUS experiment has now completed its third year of operation at the electron-proton collider HERA. The uranium/scintillator sampling calorimeter surrounding the inner tracking detectors has proven an essential component for the online triggering algorithms, for offline event-type identification, for kinematic variable reconstruction, and for a variety of physics analyses. This paper summarizes the experimental context, the operating characteristics, the calibration techniques, and the performance of the calorimeter during its first three years of operation.

1. Introduction

The uranium/scintillator sampling calorimeter for the ZEUS experiment has been operating at the electron-proton storage ring facility HERA since 1992. Its measurements of electromagnetic and hadronic shower energies, positions, and times play a central role at each of the three trigger levels, as well as in offline background rejection, event classification, reconstruction of kinematic variables, jet-finding, and a variety of other analysis tasks. It is the intention of this contribution to the conference to detail the present status of the calorimeter performance. After a review of the mechanical design, readout and calibration techniques, and selected test beam results, we concentrate on lessons learned from the first three years of operation.

2. Experimental Context

Fig. 1 depicts the general purpose, 4π -detector ZEUS designed to study the interactions of HERA's 820 GeV protons and 27 GeV electrons. The innermost component is a high resolution drift chamber (VXD) which provides transverse position measurements of track segments in a radial region from 11 to 15 cm. The central tracking detector (CTD) surrounds the vertex detector, its nine superlayers of drift cells of eight sense wires each extending from 16 to 85 cm in the radial coordinate. A superconducting solenoidal coil one radiation length (X_0) thick, providing a 1.4 Tesla field in the tracking region, is situated outside the CTD and in front of the barrel calorimeter (BCAL). In the forward (proton flight) direction a multilayer drift chamber/transition radiation detector (FDET) provides further tracking outside the CTD and in front of the forward calorimeter (FCAL). The endplate of the CTD and the

*Presented at the V International Conference on Calorimetry in High Energy Physics, Brookhaven National Laboratory, September 25 - October 1, 1994.

FDET are the dominant contributions to material between FCAL and the interaction point, consisting of $\simeq 1 X_0$. In the rear (electron flight) direction there are a small angle scintillation hodoscope (SRTD) and a planar drift chamber (RTD) in front of the rear calorimeter (RCAL). The material between RCAL and the interaction point amounts to $\simeq 0.5 X_0$, except for a narrow region near the beam pipe, where it ranges up to several X_0 . Thus over most of the detector volume the material traversed by particles before entering the calorimeter is less than $\simeq 1 X_0$, except for narrow regions near the edges of the calorimeters, where the total amount of material traversed by a straight trajectory can reach several X_0 . Surrounding the uranium calorimeter is a backing calorimeter (BAC) consisting of wire chambers installed in slots in the iron magnetic field return yoke, and the muon tracking system (FMUON, BMUON, RMUON). The forward muon system includes toroidal magnets for an additional momentum measurement. Two planes of large-area scintillation counters (Veto Wall) behind RCAL provide rejection against upstream interactions of the proton beam with residual gas in the beam pipe. A luminosity measurement is provided by small-angle electron and photon calorimeters in the HERA tunnel in the electron flight direction. A silicon-strip leading-proton spectrometer installed in Roman pots and a forward neutron calorimeter furnish information on the hadronic final state at small angles in the proton flight direction.

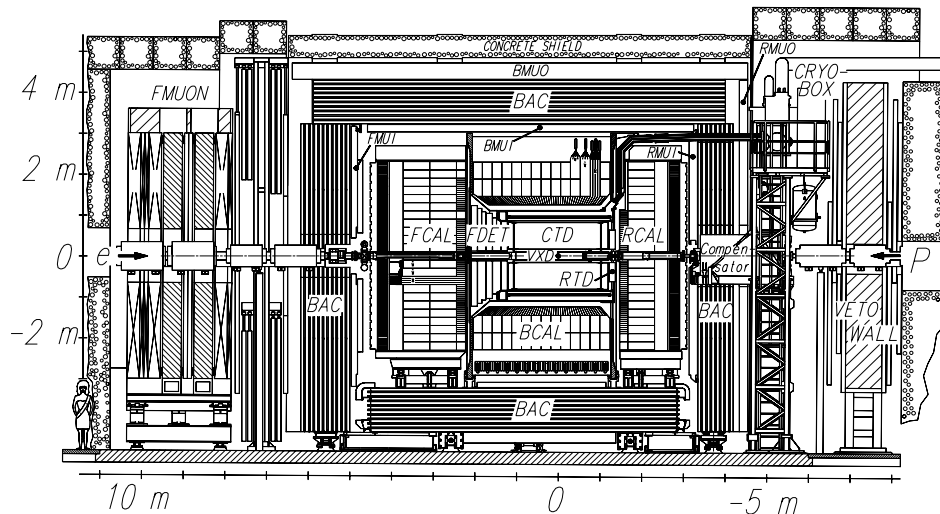


Figure 1: *The ZEUS detector*

The measurement of structure functions at the high Q^2 -values attainable at HERA requires calorimetric measurements of the scattered electron, of the hadronic final-state formed from the struck proton constituent, and of the proton remnant. The latter component of the final state is often observed as large energy depositions in FCAL near the beam pipe. In contrast, such energy depositions are conspicuously absent in such candidate events for diffractive scattering as exemplified in Fig. 2 ($Q^2 \simeq 70 \text{ GeV}^2$!). While not all diffractive scattering events show such structure,

the probability that a scatter from a colored object in the proton exhibit such an energy configuration is much less than the relative frequency with which the HERA experiments have observed such events. Particularly interesting from the point of view of calorimetry is the necessity of a low noise level in order to be able to identify events with “nothing” at forward angles. This event picture does not display signals with less than 60 MeV in electromagnetic cells and 110 MeV in hadronic cells. One observes an isolated 0.3 GeV deposit in the forward calorimeter which does not exceed the 0.4 GeV threshold used by the simple algorithm classifying this event as a candidate for diffractive scattering. This intriguing process involving a high momentum transfer scatter of the electron from an apparently colorless proton constituent is one of a wide variety of interactions which result in depositions of only a few GeV in the calorimeters.

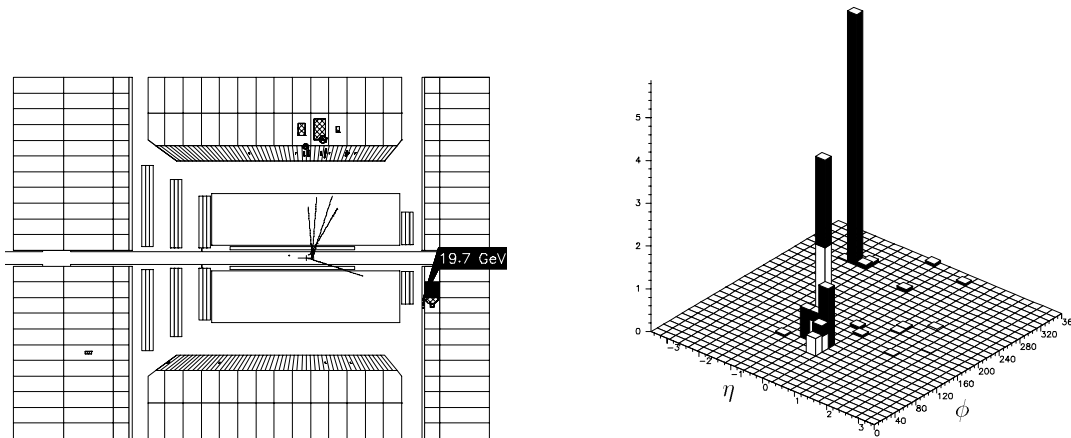


Figure 2: *Candidate Event for Diffractive Scattering at High Q^2 . The picture on the left shows tracks and energy depositions in the upper (lower) half of the detector rotated around the beam axis to the upper (lower) half of the vertical plane. The picture on the right shows a lego plot of transverse energy (GeV) in bins of pseudorapidity and azimuthal angle. Dark (light) towers represent transverse energy in the electromagnetic (hadronic) sections.*

3. Mechanical Design

The 700-ton ZEUS calorimeter^{1,2,3} consists of forward, central barrel, and rear sections, covering the polar angle ranges $2^\circ - 40^\circ$, $37^\circ - 129^\circ$, and $128^\circ - 177^\circ$. Each is made up of layers of 2.6 mm SCSN-38 scintillator and 3.3 mm stainless-steel-clad depleted-uranium plates. Each layer corresponds to $1.0 X_0$ and 0.04 interaction lengths (λ_I). This uniformity in structure throughout the entire calorimeter and the distributed nature of the natural radioactivity of the uranium are decisive factors in our ability to maintain a precise calibration of the calorimeter. The choice of active and passive thicknesses results in a sampling fraction of 4% for electromagnetic and

hadronic shower components (hence compensation⁴) and 7% for minimum-ionizing particles.

The wavelength-shifting optical readout components subdivide the calorimeters longitudinally into electromagnetic (EMC) and hadronic (HAC) sections. The EMC sections are $25 X_0$ ($1.1 \lambda_I$) deep. The FCAL (BCAL) HAC sections are further segmented longitudinally into two sections, each of $3.0 \lambda_I$ ($2.0 \lambda_I$) depth. RCAL has a single HAC section $3.0 \lambda_I$ deep. The optical components subdivide FCAL and RCAL into towers of transverse dimensions $20 \text{ cm} \times 20 \text{ cm}$. The EMC sections are further divided vertically into four (two) cells in FCAL (RCAL.) Thus the transverse segmentation of the EMC cells is $20 \text{ cm} \times 5 \text{ cm}$ in FCAL and $20 \text{ cm} \times 10 \text{ cm}$ in RCAL. The front face of FCAL (RCAL) is 2.2 m (1.5 m) distant from the nominal electron-proton interaction point. BCAL consists of 32 wedge-shaped modules situated 1.2 m distant from the beam axis. Its EMC sections are divided by the optical readout components into 53 cells per module, each of transverse dimensions $24 \text{ cm} \times 5 \text{ cm}$, approximately projective in both the polar and azimuthal angles. The fourteen HAC sections in each module measure $24 \text{ cm} \times 28 \text{ cm}$ in the transverse dimension and are projective only in the azimuthal angle. A 2.5° rotation of all the BCAL modules relative to the radial direction ensures that the intermodular regions containing the wavelength shifters do not point at the beam axis.

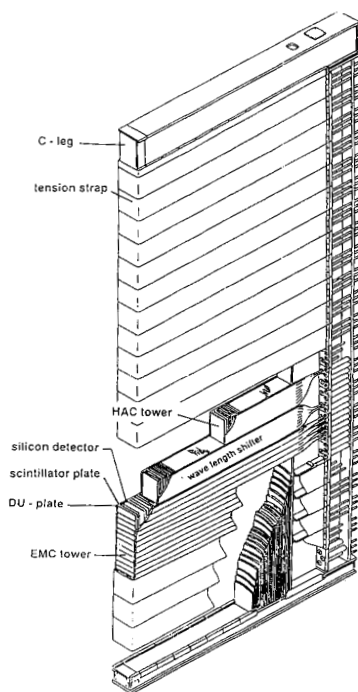


Figure 3: Geometrical configuration of an FCAL module

The light signal from each calorimeter cell is received by two phototubes which view the ends of wavelength-shifting light guides situated on opposite sides of the cell. This redundancy in the readout allows not only for a transverse position measurement within the cell, but permits the use of the left/right sum as an energy measurement independent of the impact point (which is important for the trigger), and further allows the separation of intrinsic shower fluctuations from those of photostatistical origin in beam tests. Light yield requirements imposed tight tolerances on the quality of the wavelength shifting light guides.⁵ Since they occupy “crack” regions between modules, their thickness was limited to 2 mm, the minimum consistent with constraints on the attenuation length along the length of the active area of the light guides. This source of inhomogeneity due to the attenuation was corrected with a patterned reflective wrapping. The minimum light yield is $100 \frac{\text{photoelectrons}}{\text{GeV}}$ and $1.2 \frac{\text{photoelectrons}}{\text{layer}}$ for each phototube. Thus

photostatistics contribute less than $7\%/\sqrt{E(\text{GeV})}$ to the energy resolution for electromagnetic showers, which is $18\%/\sqrt{E(\text{GeV})}$.

Fig. 3 shows the an FCAL module as an example of the above-described construction geometry. Spaces are available at depths of $3X_0$ and $6X_0$ for insertion of the $3\text{ cm} \times 3\text{ cm}$ silicon diodes (HES) which allow hadron-electron separation by sampling the electromagnetic shower near its maximum. These detectors were installed in RCAL (which has such a slot at a depth of $3X_0$ only) for the 1994 data-taking period. The FCAL HES is not yet installed.

4. Readout Technique

The phototube high voltages are set using the radioactivity of the depleted uranium. Tight tolerances during construction of the calorimeter allow the cell-to-cell variation of the response to electrons to be controlled at the 1% level when normalized to the uranium background level. The uranium calibration further determines the relative EMC/HAC phototube gains, ensuring compensation at the 1% level for shower energies exceeding 5 GeV. The compensation results in a hadronic energy resolution of $35\%/\sqrt{E(\text{GeV})}$.

The 11836 phototube signals are each split five ways in the front end analog cards: to a current integrator averaging the input current over 20 ms and providing the uranium calibration signal measurement, to a current sum node serving the first level trigger, to the two shaping-and-sampling paths of differing gains, and to a termination resistor. The shapers use precision components to define an effective shaping time constant of about 100 ns uniformly for all shapers to 0.2 ns accuracy.

The processing of the shaped signals is based on CMOS switched-capacitor chips developed for the ZEUS application.⁶ The signals are sampled at the 10.4 MHz HERA bunch crossing rate such that a sample on each of the rising and falling edges be guaranteed. A sample on the baseline preceding the pulse serves as protection against pile-up effects. The slope-weighted sum of the two baseline-corrected samples on the pulse edges provides a jitter-independent measurement of the energy deposit and the difference provides a shower time measurement. Two gain scales, differing by a factor of 22.22 (5.00) in FCAL and BCAL (RCAL), and 12-bit digitization allow an effective dynamic range of 17 (15) bits. The RMS noise level is dominated by the signal from the uranium activity and is at a level of $\simeq 10\text{ MeV}$ per cell (see section 5). The gain scales are defined such that the high gain path saturates at 24 GeV in FCAL and 18 GeV in BCAL and RCAL. The low gain paths saturate at 530 GeV in FCAL, 380 GeV in BCAL, and 90 GeV in RCAL.

Gain and pedestal correction factors are necessary for each switched-capacitor cell to ensure that noise and linearity requirements are fulfilled. These are obtained via calibration runs exploiting the on-board digital-to-analog converter (DAC) on each 12-channel front-end analog card. A complete calibration data set consists of about 20 Mbytes. The sample calibration corrections and the charge and time reconstruction algorithms are performed in digital signal processors (DSP's) treating the 12-bit

digitization results. The digitization occurs at a rate of 0.6 MHz in modules which receive the analog, multiplexed outputs of the analog cards over $\simeq 50$ m of shielded twisted-pair cable. The 58-cell pipelines are clocked continuously at 10.4 MHz until a first-level trigger occurs, at which time they are stopped for $10 \mu\text{s}$ to transfer six samples for each gain path to the switched-capacitors in a buffer-multiplexer chip. Front end data acquisition then continues while the buffer-multiplexer data is clocked at 0.6 MHz to the digitizers. This double-buffering scheme achieves a deadtime of 1% for a 1 kHz first-level trigger rate and allows $5 \mu\text{s}$ for a trigger decision.

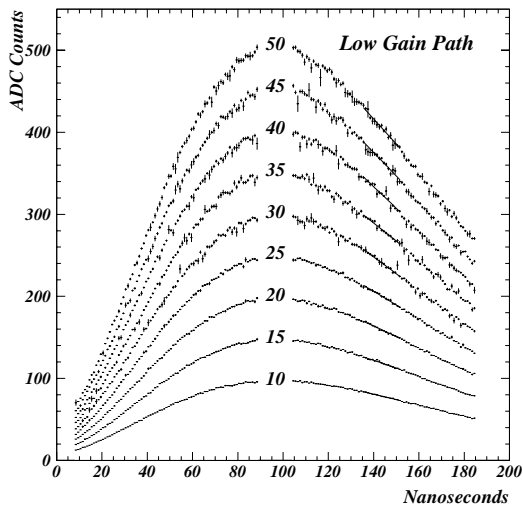


Figure 4: *Pulse shaping for electron showers between 10 and 50 GeV. The data are obtained by running the pipeline clock asynchronously and plotting sample heights (here the samples on the rising and falling edges are shown) as functions of the arrival time - clock edge time difference.*

The DSP's provide calibrated energy and time measurements to the second-level trigger transputer network, as well as to an event builder serving the third-level MIPS processor farm.

One means of measuring the pulse shape is provided by running the pipeline clock asynchronously and plotting sample heights versus the time difference between particle arrival time and pipeline clock edge. Fig. 4 shows the pulse shapes for test beam electrons between 10 and 50 GeV.

A second generation of switched-capacitor chips was installed during the shutdown preceding the 1994 data run. The new chips have been demonstrated to survive an order of magnitude greater radiation dose compared to the original generation, continuing to operate at doses up to 1000 Gray.⁷

5. Operating Characteristics

The operating characteristics of the calorimeter were determined in extensive test beam programs at FNAL and CERN^{3,8} on both prototype and final modules. Fig. 5 shows the energy dependence of the resolution and the ratio of electron to pion signals, measured in FCAL prototype modules at CERN, documenting the values cited above. The uniformity across module and tower boundaries was thoroughly investigated as well. Nonuniformities at the level of 10% occur in narrow regions near cracks, resulting in an averaged nonuniformity under 1%. Of the total of 80 modules, six FCAL, four RCAL, and six BCAL modules were examined in test beams. One goal was the verification of construction tolerances as reflected in the cell-to-cell reliability

of the uranium signal calibration. Fig. 6 shows an example of a result for 15 GeV electrons in FCAL and RCAL modules. These ten modules comprised 37% (28%) of all the electromagnetic cells in FCAL (RCAL). Cell-to-cell RMS variations of 1.3% (1.5%) were measured for these FCAL (RCAL) cells, to which the measurement uncertainty contributed 0.3%. All FCAL and RCAL modules were subsequently measured at DESY using cosmic ray muons, with such accuracy that the individual cell variations within the 1% RMS spread could be corroborated for the cells which had been measured at CERN. Of the 32 BCAL modules, 22 underwent extensive investigations with cosmic rays as well.⁹

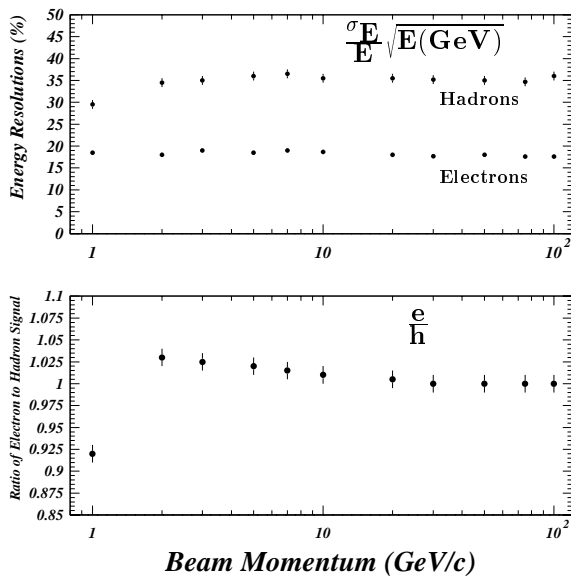


Figure 5: *Energy resolution and the ratio of electron to pion signals as a function of beam momentum, measured for the FCAL prototype modules at CERN.*

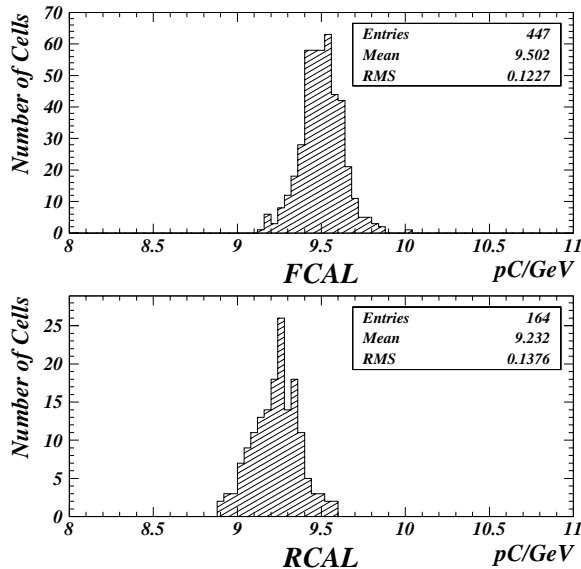


Figure 6: *Cell-to-cell calibration uniformity for the six FCAL and four RCAL modules measured at CERN. These modules comprise 37% (28%) of all the electromagnetic cells in FCAL (RCAL). RMS nonuniformities of 1.3% and 1.5% were measured.*

6. Calibration Methods

The natural radioactivity of the uranium provides the absolute calibration of the ZEUS calorimeter. Test beam studies furnished the calibration factors necessary to maintain the calibration at the level of 1%. During data-taking periods the uranium currents are recorded daily for use as offline normalisation correction factors. Fig. 7 shows measurements of the uranium current signal, averaged over 20 ms to remove statistical fluctuations, for each phototube of the central FCAL module. The nominal currents are chosen such as to ensure that the response of each cell to minimum-

ionizing particles scale with the number of layers in the cell. The factor of five greater HAC uranium signals as compared to the EMC uranium signals is the result of the larger transverse cell dimension (20×20 cm versus 5×20 cm), the larger number of uranium/scintillator layers (80 versus 25), and a thicker stainless steel cladding (400μ versus 200μ) on the uranium plates. Deviations of the uranium current settings from nominal are shown in Fig. 8 for a recent run. Of the 11836 tubes, 126 deviated by more than 20% from the nominal setting and were excluded from the offline analysis. Variations over the period of a week are typically under 1%. Adjustments of the phototube high voltage values to reestablish the nominal currents are undertaken once a month.

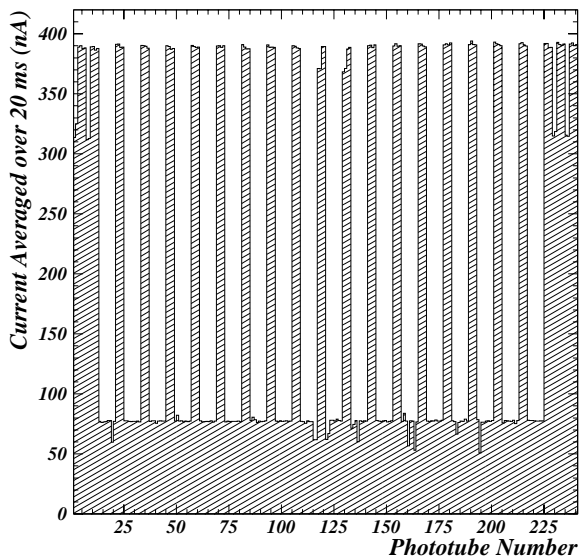


Figure 7: Uranium activity calibration current values for the central FCAL module on 1 September 1994.

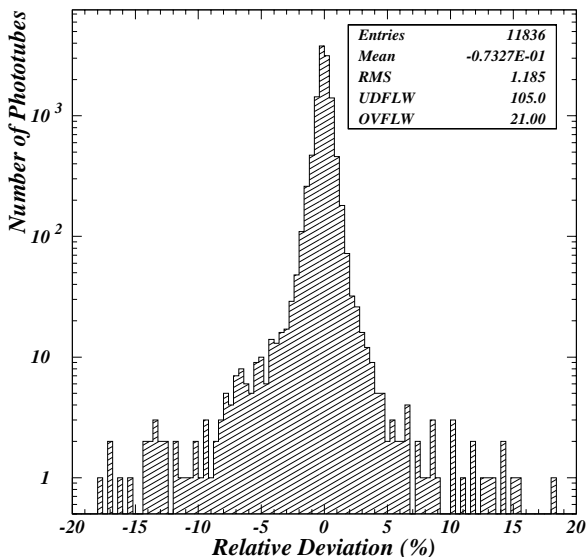


Figure 8: Relative deviations from the nominal uranium activity calibration current values for the central FCAL module on 1 September 1994.

As mentioned in section 4, the switched-capacitor readout is calibrated by means of on-board DAC's which provide levels at the inputs to the pipelines, allowing the measurement of gain and pedestal values for each capacitor. Calibrated charges are also injected at the inputs to the shapers. A complete calibration of the front-end electronics is performed once a week.

Strict rejection criteria based on the weekly front-end calibration and the daily measurements of charge injection and uranium currents are used to generate a list of channels to be excluded from the offline analysis. Typically $\simeq 2\%$ of the 11836 readout channels are declared useless. The number of calorimeter cells for which *both* readout channels malfunction at any time is typically less than two.

Each phototube is equipped with an optical fiber permitting light injection into the wavelength-shifting light guide just in front of the photocathode. The LED and laser

light sources provide periodic measurements of the gain, linearity, photostatistics, and phototube transit times.

Precise measurements of the structural integrity of the FCAL and RCAL modules are obtained by sliding a 1-mm-long 70 MBq ^{60}Co source in steps of 0.2 mm through tubes positioned along the length of a tower.¹¹ This method allows the verification of the positioning of each scintillator tile and of the wavelength-shifter assemblies. All modules were scanned before installation in 1991 and during shutdowns accessible modules in the beam pipe region have been scanned each year. The shapes of the ^{60}Co distributions have shown stability at the 2% level over a period of three years, consistent with the negligible radiation damage expected from dosimeter measurements.

7. Selected Applications in Physics Analyses

The 1994 HERA data-taking period, which ended on November 1, has provided the ZEUS experiment with 6.1 pb^{-1} of integrated luminosity, to be compared to 1.1 pb^{-1} in 1993 and 0.05 pb^{-1} in 1992. The rapid progress of the HERA accelerator performance means that our ability to study systematic effects in the calorimeter response continues to improve dramatically. The studies presented in this paper are based on the data recorded in 1992 and 1993, thus representing 15% of our entire data sample to date. We present here a selection of the applications of the calorimeter data, sorting them according to the use of the time, position, and energy measurements.

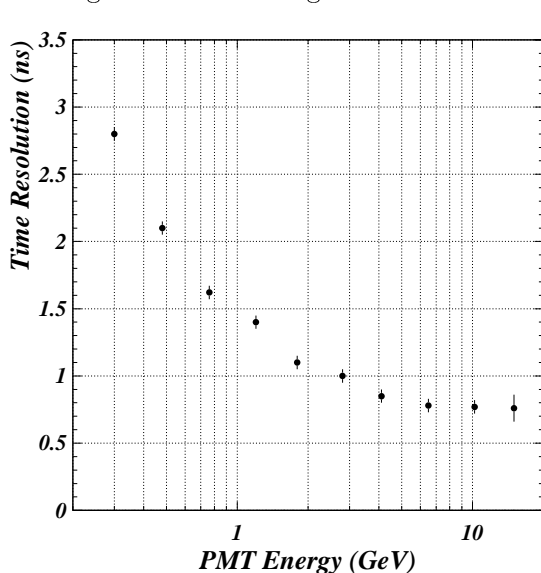


Figure 9: *Single phototube calorimeter time resolution for electromagnetic energy depositions in FCAL.*

The shaping-and-sampling algorithm described in section 4 provides measurements of the phototube pulse time relative to the pipeline clock, which is synchronized to the accelerator RF. After corrections for time shifts of the bunch arrival time relative to the HERA RF, differences in the distance of each calorimeter cell from the interaction point, shower development times, and phototube transit times, subnanosecond resolutions are obtained.¹⁰ Fig. 9 shows the time resolution for an FCAL EMC cell in an energy range where systematic effects begin to dominate the statistical and shower fluctuations. In general, one achieves a resolution of better than 1 ns for depositions greater than a few GeV per phototube.

This time information plays an important role in the rejection of triggers caused by particles produced in interactions of the proton beam with the residual gas in the

beam pipe. These upstream interactions produce depositions in the rear of RCAL, which differ in time from depositions by particles produced at the electron-proton interaction vertex by 12 ns. Since the RCAL time measurement as calculated from all RCAL energy depositions is accurate to better than 1 ns even without all the offline corrections listed above, it provides a powerful tool for background rejection at the second trigger level.

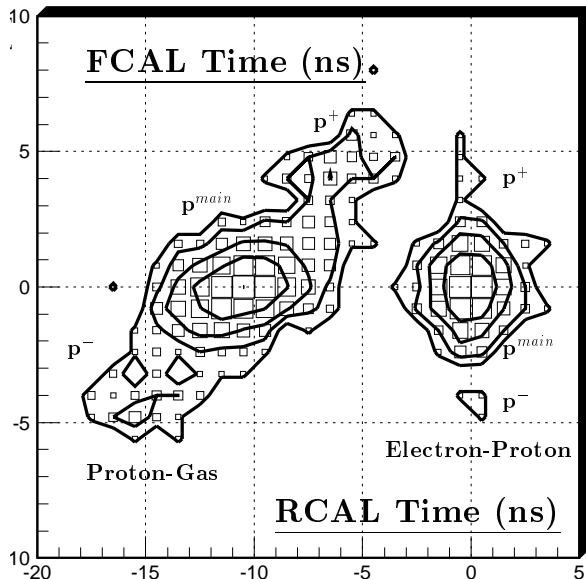


Figure 10: *Correlated FCAL and RCAL calorimeter time measurements. Contributions from proton primary (p^{main}) and satellite (p^- , p^+) bunches to both beam-gas background and electron-proton interactions are evident.*

The calorimeter event times are also used to determine the position of the interaction vertex along the beam line. While the resolution of 8 cm is an order of magnitude worse than that of the CTD, the systematics and acceptance are very different. In particular, the calorimeter measures the vertex position better than the CTD in events with tracks at small angles only.

The primary use for the calorimeter measurements of incident position is for that of the scattered electron produced in the neutral-current deeply inelastic scattering (DIS) process. The rate of the low- Q^2 electrons at small scattering angles falls steeply with scattering angle and the position cut defines the lower bound on the acceptance in Q^2 . The best estimate of the calorimeter position resolution in this region is given by comparison to position measurements calculated from the HES silicon-diode detector data in RCAL, which have a resolution better than 3 mm. The comparison indicates a resolution of 1.3 cm vertically (via charge sharing between cells) and 0.8

Another contribution of the calorimeter event time measurements is the monitoring of irregularities in the HERA beams' RF structure. In 1993 a new RF system was activated for the proton beam, reducing the primary proton bunch RMS length from 40 cm to 20 cm. Some protons were trapped in satellite bunches which lead and trail the primary proton bunch by 4.5 ns. Since the population and lifetime of these satellite bunches varied dramatically from fill to fill, monitoring their behavior and correcting the data samples for triggers caused by their interactions was essential. Fig. 10 shows a contour plot of FCAL time versus RCAL time, illustrating the time structure of the contributions from proton primary and satellite bunches to both beam-gas background and electron-proton interactions.

cm horizontally (via the transverse light attenuation in the scintillator tiles), averaged over the position and energy distributions of the scattered electrons, which peak at small scattering angles and near the electron beam energy. The position resolution varies strongly with the position within a cell and reaches an accuracy of 3 mm in the vertical coordinate near cell boundaries.

We begin our discussion of the calorimeter energy measurement with the noise levels, which are dominated by the uranium signal contribution to fluctuations in the three samples used to reconstruct the charge. Fig. 11 shows for all 11836 channels the RMS width values from pedestal triggers recorded during empty bunches of a physics run. Two bands are observed for each calorimeter, each corresponding either to the EMC or to the HAC cells. In general, the noise levels are $\simeq 10$ MeV in the EMC cells and $\simeq 15$ MeV in the HAC cells, for which the uranium currents are greater. Also shown is the noise level measured with the high voltages off, corresponding to $\simeq 5$ MeV.

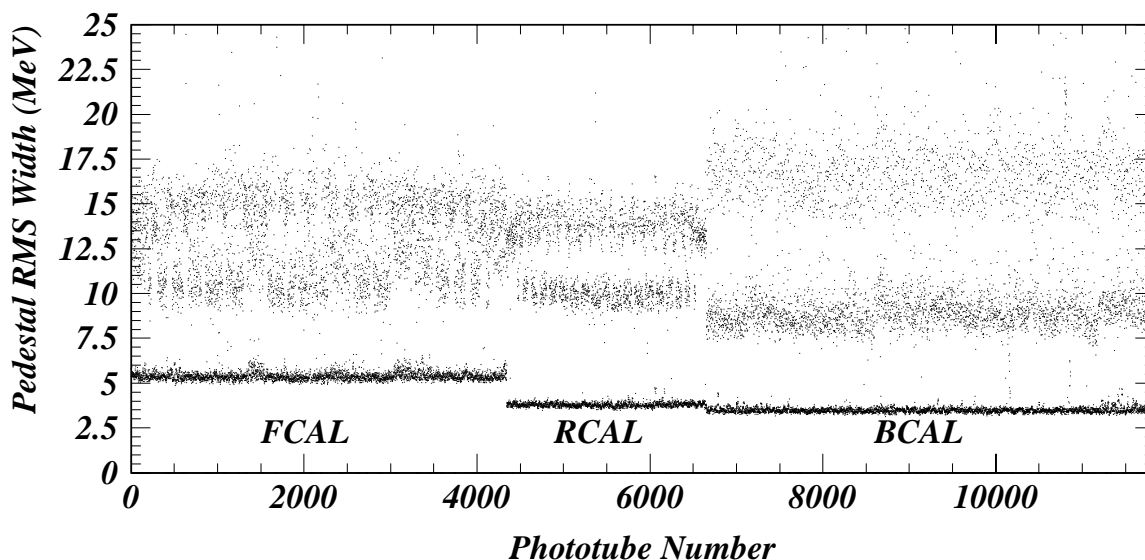


Figure 11: *Pedestal RMS width values for the 11836 phototubes as calculated from triggers recorded during empty bunches of a physics run. Bands at values of 10 MeV and 15 MeV show the levels for the EMC and HAC cells of each calorimeter. The values near 5 MeV were measured with the high voltages turned off and indicate the contribution from the electronics noise. Disfunctional readout channels ($\simeq 2\%$ of all channels) are not excluded from this plot.*

For comparison, fig. 12 shows the RCAL signal reconstructed from proton beam halo muons, which deposit 330 MeV electron-equivalent-energy in the EMC section and 1100 MeV in the HAC section, as well as the pedestal distribution for the six-channel sum for a single RCAL tower, which has an RMS width of 36 MeV. There is a slight correlation in the noise from the two phototubes of the same calorimeter cell.

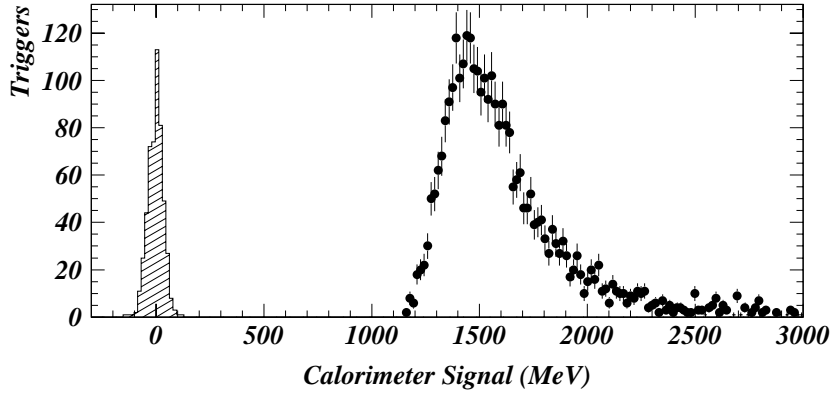


Figure 12: A comparison of the pedestal signal summed over the six channels of an RCAL tower and the pedestal-suppressed signal for the entire RCAL from beam halo muons, which deposit 330 MeV electron-equivalent-energy in the EMC section and 1100 MeV in the HAC section.

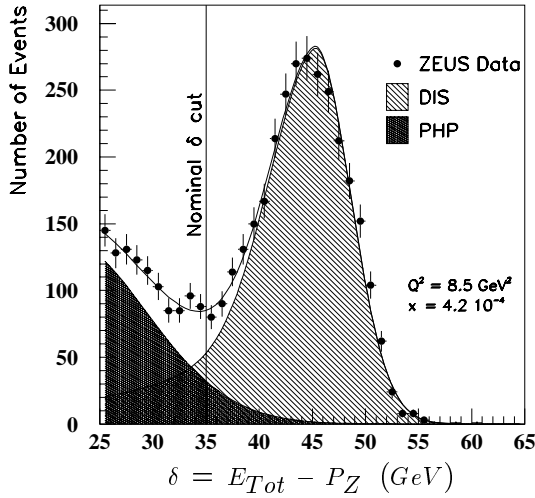


Figure 13: The distribution in the variable $\delta = E_{Tot} - P_Z$ summed over the entire calorimeter for DIS candidate events in a bin of x_{Bj} and Q^2 where the background from photoproduction processes is significant.

Fig. 13 shows how the calorimeter data contribute to the event-type selection by exploiting the longitudinal kinematic constraint for DIS events.¹² Shown is the distribution of the total energy measured in the calorimeter with the total longitudinal momentum subtracted. This quantity is insensitive to fluctuations in the energy measured in the forward direction and is kinematically constrained for DIS events to a value of twice the electron beam energy. For the present purpose of illustration, a region of x_{Bj} and Q^2 has been chosen such that the background from photoproduction processes, where the electron exits the detector through the beam pipe, is significant.

The DIS contribution is observed to peak near 45 GeV rather than at the value of 54 GeV expected if sources of signal loss are ignored. The kinematic constraint is compromised by energy loss of both the electromagnetic and hadronic final state in dead material between the interaction point and the calorimeter.

The energy-loss correction algorithms under development will not be discussed in this paper, however two observations are appropriate. The first is that studies using the proton beam halo muons mentioned above and comparing their signals with both the cosmic ray data and the test beam data verified the energy scale calibration of the calorimeter with an accuracy of 3%. Secondly, the SRTD, which covers an area of 4500 cm^2 around the beam pipe in front of RCAL, has proven to provide an accurate means of correcting for early showering. The depositions in these strips exhibit an anticorrelation to the calorimeter signal, as shown in fig. 14 for a sample of DIS electrons in which the scattered electron energy is constrained to the beam energy. The selection of these electrons exploits the overconstrained kinematics, deriving the electron energy from its angle and the hadronic final state. The distribution of selected energies has an asymmetric tail due to radiation by the initial state electron and to the resolution in the cut variables. The simple linear correction function depicted in the upper left-hand plot in fig. 14 results in the improvement indicated in the lower right-hand plot. The SRTD was installed during the 1993/1994 shutdown and such studies are just now becoming available.

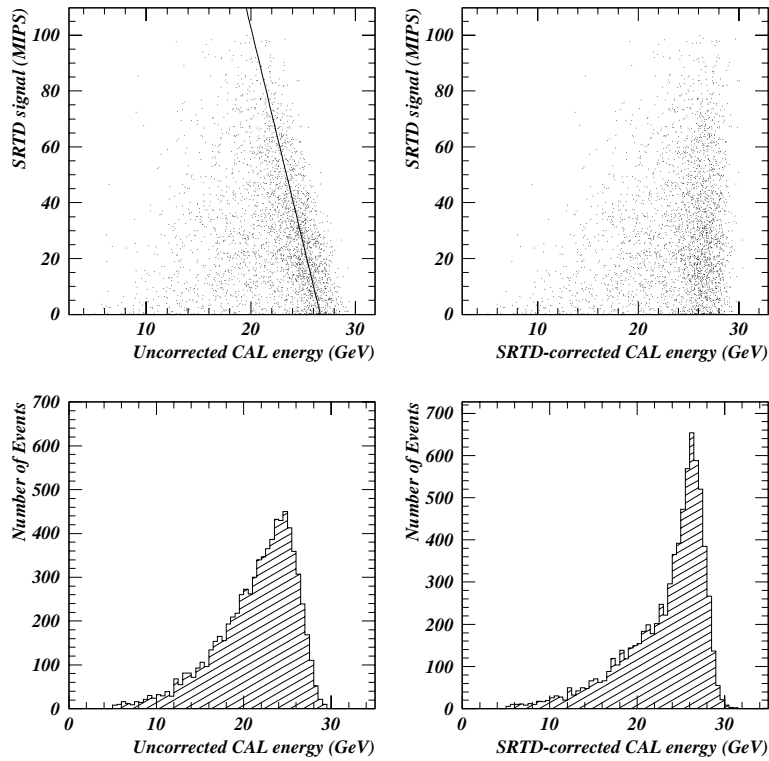


Figure 14: A correction procedure for energy loss in material in front of RCAL using presampling by the SRTD for scattered electrons kinematically constrained by selection to the electron beam energy. The simple linear correction function derived from the anticorrelation of the SRTD and RCAL signals shown in the upper left-hand figure results in the improved spectrum indicated in the lower right-hand figure.

8. Upgrades in Progress

A presampling detector component consisting of $20 \times 20 \text{ cm}^2$ scintillator tiles read out via wavelength-shifting fibers and covering the portions of the faces of FCAL and RCAL which are not shadowed by BCAL was approved early this year for installation during the 1994/1995 shutdown. The proposal for this detector was based on test beam studies performed in 1992 and 1993 which indicated that an energy correction algorithm was practical. In particular, it was shown that the correction could be made independent of specific knowledge of the presence of dead material in front of the presampler up to $4 X_0$ and that an event-by-event correction brought substantially more improvement than an average correction based on the geometry of the dead material.¹³ Further analyses of test beam data recorded in 1994 are in progress.

Preparations for the installation of the HES silicon-diode detectors in FCAL, complementing those installed in RCAL in 1994, are underway. Pilot modules will be instrumented for the 1995 data-taking period, with full instrumentation of one slot approved for the following year.

Initial simulation and test beam studies have been undertaken for barrel presampler and shower-max detectors. A proposal for this upgrade is in preparation.

A redesign of the beam pipe which will reduce the dead material in front of RCAL for small electron scattering angles has been concluded. Construction is underway and installation is expected for the 1994/1995 shutdown.

9. Summary

The performance of the ZEUS uranium/scintillator sampling calorimeter during the first three years of HERA operation has been consistent with design parameters and expectations gained from test beam measurements. The use of the natural radioactivity of the uranium has proven to be a simple and reliable calibration technique. To date no aging effects inconsistent with the design lifetime of ten years have been observed.

The calorimeter measurements of energy, position, and time play critical roles at each of the three trigger levels, in the event classification algorithms, and in the physics analyses. A spatial resolution of 1 cm and a time resolution of 0.5 ns are typical for the inelastically scattered electrons produced in neutral-current interactions at HERA. The hadronic and electromagnetic energy measurements are degraded at a level of up to $\simeq 20\%$ by material of thickness ranging up to several radiation lengths between the calorimeter and the interaction vertex in narrow angular regions. The use of presampling techniques in test beam measurements and in situ show results encouraging for energy correction algorithms. A full-scale presampler for the forward and rear calorimeters will be installed prior to the 1995 data-taking period.

10. Acknowledgements

I acknowledge with pleasure the support of the ZEUS calorimeter group during the preparation of this paper, in particular the extensive advice received from Uli Kötz. My colleagues Erwin Hilger and Uli Katz provided constructive commentary based on their critical readings of drafts. This work further profited from productive discussions with Allen Caldwell, Mark Lancaster, Thomas Neumann, Johnny Ng, Ruben Schattevoy, Tatsu Tsurugai, Wouter Verkerke, and Marcel Vreeswijk.

11. References

1. The ZEUS Detector, Status Report 1993, DESY 1993.
2. M. Derrick et al., NIM A309 (1991) 77.
3. A. Andresen et al., NIM A309 (1991) 101.
4. H.Brückmann et al., NIM A263 (1988) 136.
R.Wigmans, NIM A259 (1987) 389.
J.E.Brau and T.E.Gabriel, NIM A238 (1985) 489.
5. J.Hartmann et al., NIM A305 (1991) 366.
B.G.Bylsma et al., NIM A305 (1991) 354.
6. A.Caldwell et al., NIM A321 (1992) 356.
A.Caldwell et al., DESY 92-130 (1992).
L.Hervas, Ph.D. Thesis U.A.Madrid, DESY F35D-91-01 (1991).
W.Buttler et al., NIM A277 (1989) 217.
W.Sippach et al., IEEE-NS 36 (1989) 465.
7. A.Caldwell et al., DESY 92-130, 2nd Annual Conference on Electronics for Future Colliders (1992).
8. A.Bernstein et al., NIM A336 (1993) 23.
A.Andresen et al., NIM A290 (1990) 95.
U.Behrens et al., NIM A289 (1990) 115.
R.Klanner, NIM A265 (1988) 200.
9. U.Behrens et al., NIM A339 (1994) 498.
I.Ambats et al., NIM A320 (1992) 161.
10. R.Schattevoy, Ph.D. Thesis U.Bonn, BONN-IR-94-08 (1994).
11. U.Behrens, et al., NIM A323(1992) 611.
12. M.Derrick et al., *Measurement of the Proton Structure Function F_2 from the 1993 HERA Data*, DESY 94-143, submitted to Z. Phys. C.
13. H.Grabosch et al., NIKHEF-H-93-11 (1993).